scientific reports

Check for updates

OPEN

Superconducting and charge-ordered states in the anisotropic *t–J–U* model

Yifan Feng, Jie Lou & Yan Chen✉

Motivated by the effect of symmetry breaking in cuprates superconductors $YBa_2Cu_3O_{7-\delta}$, we employ the renormalized mean-field theory to study the presence of uniform superconducting and charge-ordered states in two anisotropic *t–J–U* models, either with hopping strength anisotropy or antiferromagnetic interaction anisotropy. In the case of uniform superconducting state, compared with the isotropic *t–J–U* model with only $d_{x^2-y^2}$-wave superconducting state, there is an additional *s*-wave superconducting state in the model with hopping strength anisotropy. Meanwhile, the hopping anisotropy may enhance the critical Coulomb interaction U_c at the Mott insulator to the Gossamer superconductor transition point, and strong hopping anisotropy may weaken the superconducting state. In the case of a charge-ordered state, hopping anisotropy may suppress the amplitude of the charge density waves and pair density waves, which originate from local Coulomb interactions. These results indicate that the effects of hopping anisotropy and local Coulomb interactions are competitive. Moreover, the antiferromagnetic interaction anisotropy only weakly suppresses the superconducting gap and density wave amplitude. Our results show that the *t–J–U* model with hopping anisotropy is qualitatively consistent with experimental superconducting pair symmetry and charge density waves in the $YBa_2Cu_3O_{7-\delta}$ system.

Due to the strong correlations between charge and spin degrees of freedom, high-temperature cuprate superconductors exhibit exotic physical properties[1,2]. The electronic and magnetic properties of these materials have been studied extensively, with the primary role played by the common CuO_2 plane. Among these cuprate superconductors, $YBa_2Cu_3O_{7-\delta}$(YBCO) material has a one-dimensional CuO chain to the prevalent two-dimensional CuO_2 plane. Meanwhile, many experiments revealed the physical properties with anisotropy of YBCO via Nernst[3,4], transport[5] and inelastic-neutron-scattering measurements[6]. Therefore, its pairing symmetry and charge order differ from materials without a CuO chain. Angle-resolved photoelectron spectroscopy[7,8], inelastic light scattering[9] and phase-sensitive measurement[10,11] show that the superconducting energy gap will vary in different directions due to lattice anisotropy, giving $(d_{x^2-y^2}+s)$-wave superconducting pairing. Another class of states of interest in the underdoped to the optimal doping region is called charge order states. X-ray scattering[12–14], X-ray diffraction[15–17], and sound velocity measurements[18] experiments support the presence of an incommensurate charge density wave (CDW) state with a wave vector around 0.31 in YBCO, which is different from the commensurate charge density wave with a wave vector of 0.25 in lanthanum-based "214"-type cuprates[19–23].

The CuO_2 plane plays an essential role in the formation of superconductivity in cuprates, and its fundamental features can be described by the *t–J* model[24,25]. The projection operator in the *t–J* model excludes double occupancy at one site, reflecting a strong correlation effect. In particular, Gutzwiller approximation in renormalized mean-field theory (RMFT)[26] uses statistical weight factors to handle the projection operator, and $d_{x^2-y^2}$-wave superconducting state and some charge-ordered states have been found[27–31]. As an effective model in the strong U limit of the Hubbard model, the *t–J* model serves as a minimal model to describe the high-temperature superconductivity. However, in cuprates, the ratio of Coulomb interaction to bandwidth deviates from the strong correlation limit, and the possibility of double occupancy cannot be excluded entirely. Therefore, it is necessary to consider the *t–J–U* model[32,33], which contains both the kinetic energy term, superexchange term, and the on-site Coulomb repulsion term. It can describe a weak and intermediate interacting strength system. When $U=0$, it corresponds to noninteracting tight-binding model, and in the limit $U\to\infty$, it is reduced to the *t–J* model. Several methods are used to solve this model, such as variational Monte Carlo[34], RMFT[34–36], density matrix renormalization group[32,37] and diagrammatic expansion Gutzwiller wave-function method[38,39]. Compared with the experimental data, the *t–J–U* model is more suitable than the *t–J* model to describe cuprates[38].

Department of Physics and State Key Laboratory of Surface Physics, Fudan University, Shanghai 200433, China. ✉email: yanchen99@fudan.edu.cn

Several models have been proposed to describe the electronic states in YBCO materials, such as the multi-band model containing CuO_2 planes with CuO chains[40–44]. Considering the orbital hybridization between the plane and the chain, the multiband model can be reduced to an anisotropic t–J model in the CuO_2 plane[45–50]. To describe the anisotropy in YBCO materials more precisely, we consider two anisotropic t–J–U models in this paper and use the RMFT method to study the superconducting pair symmetry and charge-ordered states. We find $(d_{x^2-y^2}+s)$-wave superconducting state consistent with the experiment and two CDW states accompanied by pair density wave (PDW). One is the antiphase charge density wave (AP-CDW) state with alternating positive and negative pair field distribution. Moreover, the other is the nodal pair density wave (nPDW) state with a non-zero net pairing field. Both density wave states are suppressed with the enhancement of the hopping anisotropy. We also calculate the local density of states (LDOS) in the nPDW states, obtain the strength of superconducting coherence D, and find that it oscillates synchronously with the hole density in real space.

Results

Hopping anisotropy

Phase diagram of superconducting state

As mentioned above, we use anisotropic t–J–U models to study superconducting and charge-ordered states in YBCO materials. RMFT has been applied to analyze strongly correlated electrons. We introduce four variational order parameters, electron density n_i, doublon density d_i, pairing field $\Delta^{\nu}_{ij\sigma}$, and bond field $\chi^{\nu}_{ij\sigma}$. Details are discussed in "Methods" section. First, we focus on the uniform state in the anisotropic hopping model at the half-filled case. Figure 1 shows the phase diagram in the parameter space U and t_y/t_x. The horizontal axis is Coulomb repulsion, reflecting the strength of the correlation, and the vertical axis is the ratio of the hopping in the y direction to the hopping in the x direction, reflecting the hopping anisotropy. When $t_y/t_x = 1$, it is an isotropic t–J–U model, and d-wave pair state appears at $U < 10.23$. In real space, the superconducting gap in the x and y directions are equal in size and opposite in sign.

When the anisotropy of the hopping strength is small, and the Coulomb repulsion weakens, an admixed $d_{x^2-y^2}+s$ pair state will appear in the system. This is because the anisotropy hopping makes the superconducting gap unequal in the x and y direction, which is consistent with the existence of $(d_{x^2-y^2}+s)$-wave superconductivity in anisotropy $YBa_2Cu_3O_{7-\delta}$. Gradually increasing the anisotropy of the hopping strength, the superconducting state is suppressed. Still, there is a finite effective carrier density d, and finally, a second-order phase transition occurs and transforms into a metallic state. When the hopping anisotropy is small and the Coulomb repulsion gradually increases, the first-order phase transition between the superconductor and insulator occurs, and the system enters the strong correlation region from the weak correlation region. It is noted that anisotropy will delay the system from the superconducting phase to the insulating phase, that is, the increase of U_c. To a certain extent, there is a competitive effect between the influence of hopping anisotropy and Coulomb repulsion on uniform state.

In Fig. 2, we show the doublon density for different hopping strength anisotropy as a function of Coulomb repulsion at half-filling. When $t_y/t_x = 1$, the doublon density decreases continuously with the increase of the Coulomb repulsion until $U_c = 10.23$ and tends to a finite value $d_c = 0.02$. Then the doublon density jumps to zero, and the model is equivalent to the t–J model, indicating a first-order Mott transition at this time. When the Coulomb repulsion weakens, the variation trends of doublon density with Coulomb repulsion are the same under different anisotropy. When the Coulomb repulsion reaches the vicinity of U_c, as the hopping strength anisotropy increases, U_c also increases, and the existing area of the Gossamer superconducting state become wider. Meanwhile, the doublon density discontinuity becomes smaller and tends to change continuously to zero, weakening the first-order phase transition characteristics. It is noted that when $t_y/t_x = 1.27$, there is a phase transition from metallic phase to superconducting phase and finally to Mott insulating phase in the system with the increase of U. When the phase transition from metallic state to superconducting state occurs, the variation trend of doublon density does not change, which is a second-order phase transition.

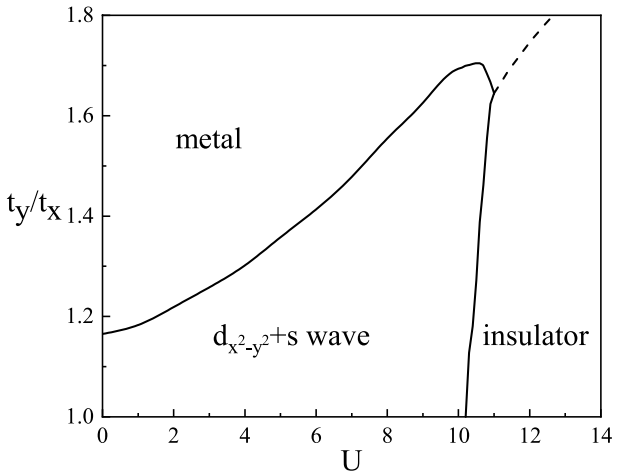

Figure 1. Phase diagram at half-filling.

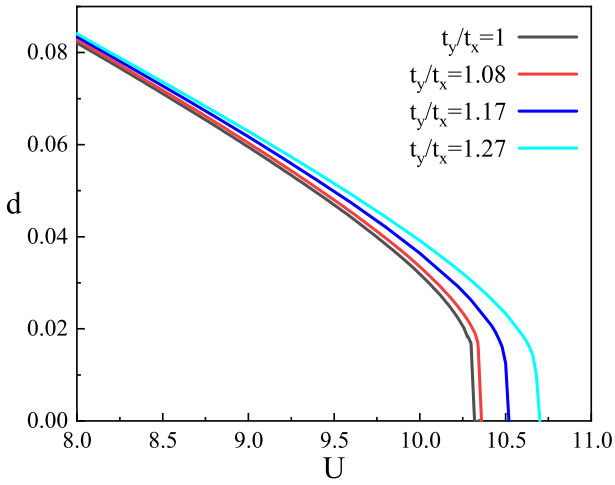

Figure 2. The doublon density d as a function of U at half-filling.

In Fig. 3a, we show $d_{x^2-y^2}$-wave superconducting gap Δ_d and s-wave superconducting gap Δ_s as a function of anisotropy parameter t_y/t_x for $U = 9$. With the increase of t_y/t_x, Δ_d decreases, but Δ_s gradually increases from zero to a maximum value and then decreases again. Δ_s reaches its maximum at $t_y/t_x = 1.17$ and $\Delta_s/\Delta_d = 0.09$. The ratio of s-wave to $d_{x^2-y^2}$-wave gap is consistent with the phase-sensitive experimental results[10]. When $t_y/t_x > 1.8$, Δ_d and Δ_s decrease smoothly to zero. However, the superconducting gap in the x and y directions always decreases with increasing hopping anisotropy. Excessive hopping anisotropy may lead to the gap closing prematurely in one direction. Figure 3b shows Δ_d and Δ_s as a function of Coulomb repulsion U for $t_y/t_x = 1.17$. As U increases, Δ_s and Δ_d reach a maximum value at $U = 9.4$ and $\Delta_s/\Delta_d = 0.09$ discontinuously decrease to zero at $U_c = 10.52$, with the same trend as the order parameter in the isotropic t–J–U model. There is a first-order phase transition from the Gossamer superconductor to the Mott insulator at U_c. It can be seen that the anisotropy hopping t–J–U model can well describe superconducting pairing symmetry and gap size of YBCO materials.

Charge-ordered state

Next, we focus on the charge-ordered state. In the t–J–U model, charge-ordered states appear at $U > 9$, commensurate and incommensurate charge-ordered states originating from local Coulomb interactions are strongly suppressed at the region where anisotropy appears. Unlike the $(d_{x^2-y^2}+s)$-wave pair in the uniform state in the hopping anisotropy t–J–U model, there is only the d-wave gap with spatial modulation, and the s-wave gap is almost zero.

When t_y/t_x anisotropy is considered, in the strongly correlated region $U > 9$, there are also the AP-CDW state and nPDW state similar to that in the isotropic t–J–U model. There are two effective carrier doublon d_i and hole h_i in the model, and the relationship with the doping density δ_i is $h_i = 1 - n_i + d_i = \delta_i + d_i$. In the strong correlation region $U = 15$, we first present the AP-CDW state results at doping density $\delta = 0.12$ in Fig. 4.The modulations are unidirectional stripe pattern which is along y direction. Figure 4d shows a schematic illustration of modulations for AP-CDW. Figure 4a shows the variation of doublon density d_i at lattice sites $i = 1$ to $i = 17$, and Fig. 4b shows the variation of hole density h_i at the same sites. The modulation of d_i and h_i have the same period of 4, and they change synchronously. Figure 4c shows the variation of gap order parameter Δ_i at the same

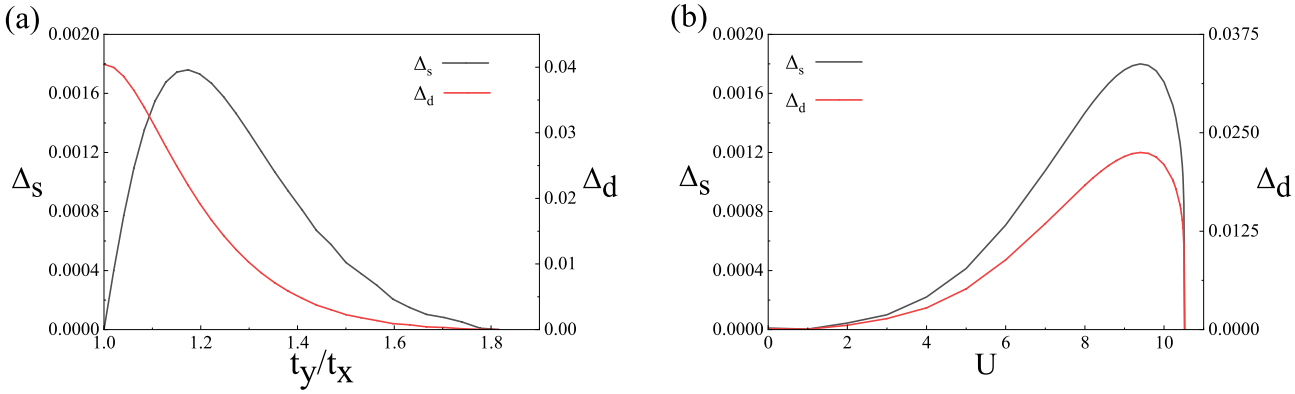

Figure 3. Superconducting order parameter (**a**) superconducting order parameter with $d_{x^2-y^2}$-wave Δ_d and s-wave Δ_s as a function of anisotropy t_y/t_x for $U = 9$. (**b**) superconducting order parameter with $d_{x^2-y^2}$-wave Δ_d and s-wave Δ_s as a function of Coulomb repulsion U for $t_y/t_x = 1.17$.

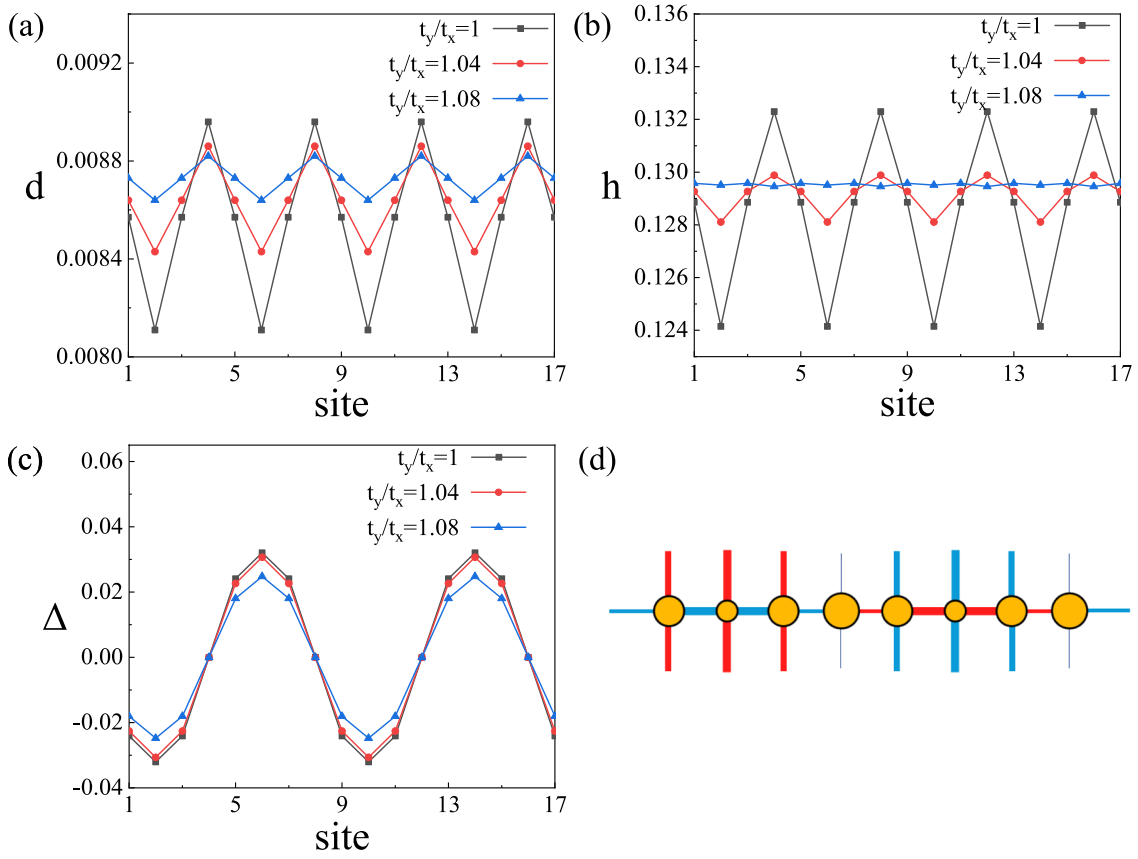

Figure 4. Features of the AP-CDW state at $U = 15$ and $\delta = 0.12$. The spatial variations of (**a**) doublon density, (**b**) hole density, and (**c**) superconducting order parameter in the system with lattice sites 1–17 in x direction. (**d**) Schematic illustration of modulations for the AP-CDW state. The diameter of the orange circles indicates the local hole density. The width of a bond around each site indicates the local pairing field and sign is positive (negative) for red (blue).

sites, and it has a period of 8 twice that of d_i and h_i. The gap order parameter changes sign once every half period. Moreover, the system has domain walls where the gap order parameter vanishes, and doublon and hole reach a maximum. In this case, the net pairing is 0. The very similar behavior of d_i and h_i originates from the strong correlation effect in the system, indicating the duality of doublon and hole. With the enhancement of hopping anisotropy, the oscillations of both charge and pair density wave states are significantly suppressed, and the suppression of hole and doublon fluctuations is more substantial. Still, the modulation period is not changed, and eventually, the system enters a uniform state. Density wave states originate from stronger Coulomb interactions, while hopping anisotropy can destroy density wave states, indicating that the effects of hopping anisotropy and correlation compete with each other.

When the hopping strength anisotropy is introduced, the nPDW state also exists in the system, as shown in Fig. 5. In this case, the spatial modulation of the charge density wave and the pair density wave is incommensurate. Figure 5d shows a schematic illustration of modulations for nPDW. Figure 5a,b show the local density δ_i, Δ_i, d_i and h_i at lattice sites $i = 1$ to $i = 21$. The system has a more complex density wave modulation. δ_i, d_i and h_i are modulated synchronously. They reach the maximum and minimum values at the same time. And Δ_i drops near zero where δ_i, d_i and h_i reach the maximum. $\delta(q)$ and $\Delta(q)$ in Fig. 5c are the Fourier transform of δ and Δ. Furthermore, the spatial average value of the superconducting order parameter is not zero, that is, $\Delta(q = 0) \neq 0$ after Fourier transform. The superconducting order parameter $\Delta(q)$ peaks at $q = 0.15$, and the doping density $\delta(q)$ peaks at $q = 0.3$, which is close to the experimentally observed YBCO charge density wave vector of 0.31[15]. Similarly, when the hopping anisotropy is too strong, the nPDW state is destroyed, and the system returns to the uniform state. With the increase of anisotropy t_y/t_x, the pairing field in the y direction decreases, leading to a transition from density wave state in the x direction to the uniform state.

We also give the local density of states $\rho(E)$ and superconducting coherence strength $D(E)$ of nPDW states at lattice sites $i = 14$ to $i = 16$ after introducing hopping strength anisotropy, as shown in Fig. 6. At site $i = 14$, δ_i, d_i and h_i reach the minimum, and the amplitude of Δ_i reach the maximum. At site $i = 16$, δ_i, d_i and h_i reach the maximum, and the amplitude of Δ_i is close to zero. Due to the $d_{x^2-y^2}$-wave pairing symmetry and the existence of the non-zero component of the superconducting order parameter at $q = 0$, the LDOS exhibits a V-type structure near the Fermi energy and remains non-zero at $E = 0$. It first decreases, then increases, and then decreases with the change of the lattice position, which has the same modulation as the hole density. The strength of superconducting coherence can be characterized by the negative of the second derivative of the LDOS

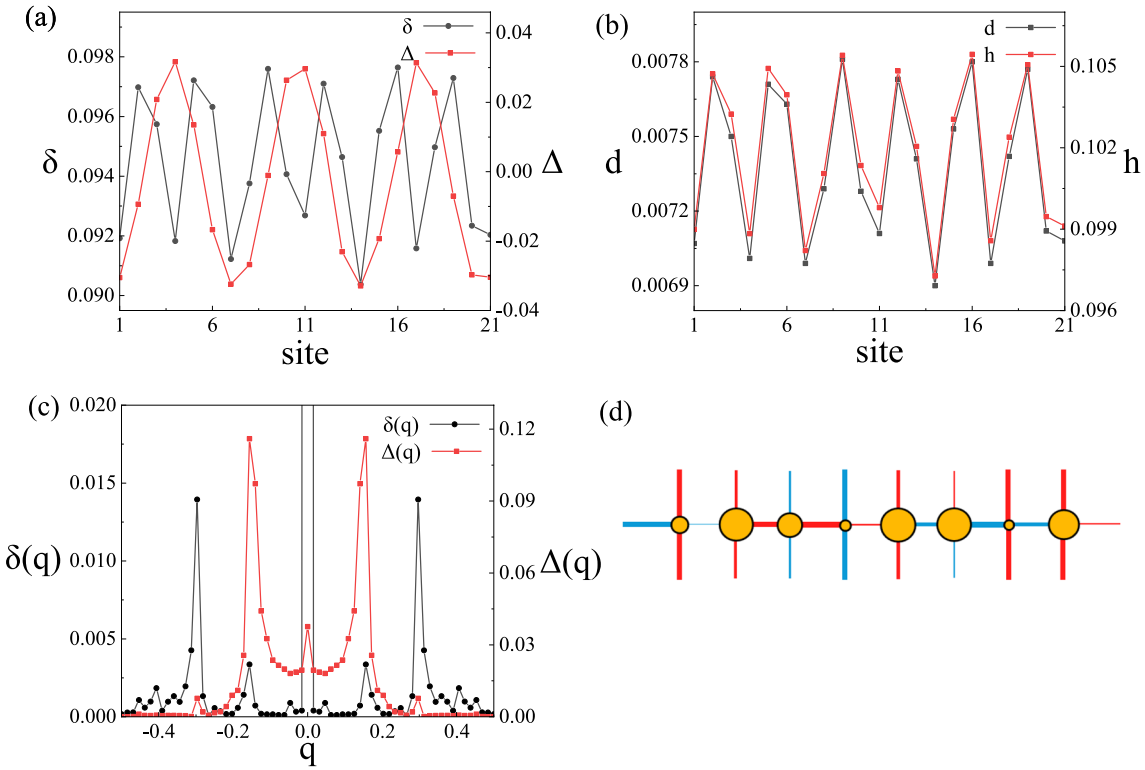

Figure 5. Features of the nPDW state at $t_y/t_x = 1.08, U = 15$ and $\delta = 0.094$. The spatial variations of (**a**) a variation of doping density (δ, left axis) and superconducting order parameter (Δ, right axis) with lattice sites 1–21 in x direction. (**b**) A variation of doublon density (d, left axis) and hole density (h, right axis) with lattice sites 1–21 in x direction. (**c**) Fourier transform of hole density and superconducting order parameter. (**d**) Schematic illustration of modulations for the nPDW state. The diameter of the orange circles indicates the local hole density. The width of a bond around each site indicates the local pairing field and sign is positive (negative) for red (blue).

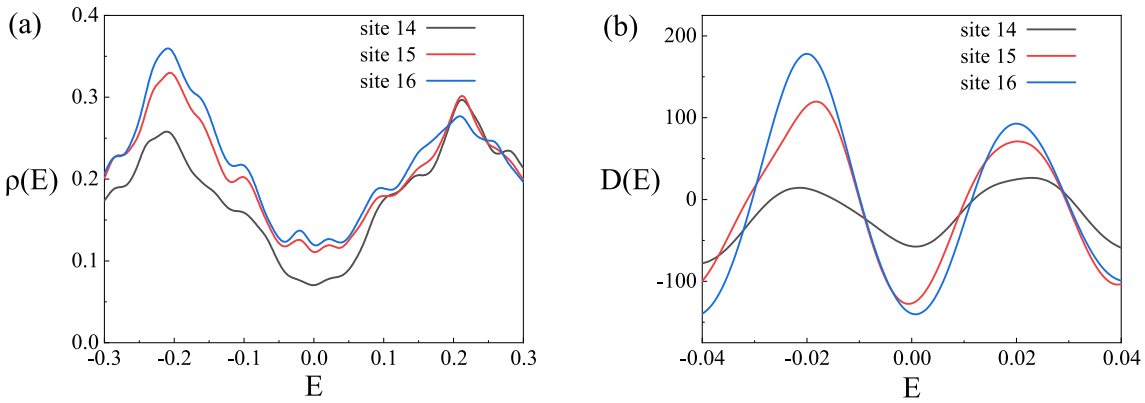

Figure 6. Features of the nPDW state at $t_y/t_x = 1.08, U = 15$ and $\delta = 0.094$. (**a**) Local density of states $\rho(E)$ as a function of E at sites 14–16. (**b**) The strength of superconducting coherence $D(E)$ as a function of E at sites 14–16 in the system.The amplitude of Δ_i reaches maximum at site 14 and close to zero at site 16.

$D(E) = -\rho''(E)$[36]. The height of the peak reflects the sharpness of the superconducting coherence peak, and it has the same modulation with δ_i, d_i, and h_i. From sites 14 to 16, the peak height and δ_i increase simultaneously.

Antiferromagnetic interaction anisotropy

In addition to the novel physics due to the hopping anisotropy in real space, we further consider intrinsic anisotropy in spin space as a theoretical conceptual extension of the t–J–U model, which breaks SU(2) symmetry. In this section, we consider the anisotropic antiferromagnetic interaction model. Now we study the uniform states in the t–J–U model with antiferromagnetic interaction anisotropy. Compared with the results of the isotropic t–J–U

model, the pairing symmetry and critical correlation strength U_c of the superconducting phase are virtually not changed. There is still a pure $d_{x^2-y^2}$-wave gap in the system, and the magnitude of antiferromagnetic interaction anisotropy only changes the gap size. The variation of $d_{x^2-y^2}$-wave superconducting gap with the anisotropy of the antiferromagnetic interaction is shown in Fig. 7. The width of the superconducting gap varies with J_z/J_x in a small range, and superconducting gap reaches its maximum as the anisotropy disappears. In the t–J–U model, the influence of antiferromagnetic interaction anisotropy on the superconducting state is far less than that of hopping anisotropy and Coulomb repulsion strength. So the antiferromagnetic interaction anisotropy does not play a dominant role in uniform states. For the superconducting state in YBCO materials, the t–J–U model with antiferromagnetic interaction anisotropy does not represent the basic features.

Next, we consider the effect of antiferromagnetic interaction anisotropy on charge-ordered states. The parameters of the pair density wave and the charge density wave states are shown in Fig. 8. Figure 8a shows the variation of doublon density d_i, Fig. 8b shows the variation of hole density h_i, and Fig. 8c shows the variation of gap order parameter Δ_i. There are charge-ordered states similar to the t–J–U model with hopping anisotropy, pair density wave state with a period of 8 and charge density wave state with a period of 4, and pairing symmetry is $d_{x^2-y^2}$-wave. Schematic illustration of modulation is similar to Fig. 4d. Hole and doublon are also modulated synchronously, and the density wave state is suppressed when antiferromagnetic interaction anisotropy is introduced. Due to symmetry, there is a similar modulation amplitude for pair density waves state when $J_z/J_x = J_x/J_z = 0.85$, while charge density waves state are symmetric concerning $J_z/J_x = 1$. In the limit case $J_z/J_x = 0$, density wave states are significantly suppressed, and only the uniform state exists. The amplitude of density wave states changes slowly with J_z/J_x, and the influence of antiferromagnetic interaction anisotropy on density wave states is weaker than that of hopping anisotropy. Moreover, the influence of antiferromagnetic interaction anisotropy on density wave states is weaker than that of hopping anisotropy. There is no density wave state with wave vector $q = 0.3$.

Conclusion

To describe the lattice anisotropy induced by CuO chains in YBCO materials and magnetic anisotropy, we study the t–J–U model with hopping strength anisotropy and antiferromagnetic interaction anisotropy in the framework of the renormalized mean-field theory. For the hopping strength anisotropy model, the superconducting pairing symmetry is still dominated by the $d_{x^2-y^2}$-wave, but with the deviation of the isotropic t–J–U model, the system will gradually have the pairing symmetry of the s-wave, and the ratio of s-wave to $d_{x^2-y^2}$-wave gap is $\Delta_s/\Delta_d = 0.09$. The t–J–U model with hopping strength anisotropy can explain the pairing symmetry of the YBCO materials, compared with the experimental results[10]. Although $(d_{x^2-y^2} + s)$-wave superconducting state is induced by the presence of anisotropic hopping, the superconducting gap decreases with the increase of hopping anisotropy. The study of the three-band model through the diagrammatic expansion of the Gutzwiller wave function method also confirmed that there is a mixed d- and s-wave pairing when the four-fold rotational symmetry is broken[51]. In the case of large U, there are charge-ordered states in the t–J–U model with hopping anisotropy, which are AP-CDW and nPDW states. The nPDW state wave vector is in good agreement with the experiment[15]. Moreover, the hopping anisotropy significantly inhibits the amplitude of charge-ordered states. In this case, the suppression mechanism of hopping anisotropy on the charge-ordered states is similar to that of the superconducting state, which inhibits the amplitude of the density waves by weakening the pairing field in y direction. Recent experiments have found that applying uniaxial stress to cuprates distorts the structure and reduces CDW order[52,53], similar to our calculations. This shows that uniaxial stress can also tune the hopping anisotropy t_y/t_x.

Further taking the intrinsic magnetic anisotropy into account, the t–J–U model with antiferromagnetic interaction anisotropy shows no new results. The effect of antiferromagnetic interaction anisotropy on the superconducting state is not very strong in the case of small U but makes the superconducting gap fluctuate in a small

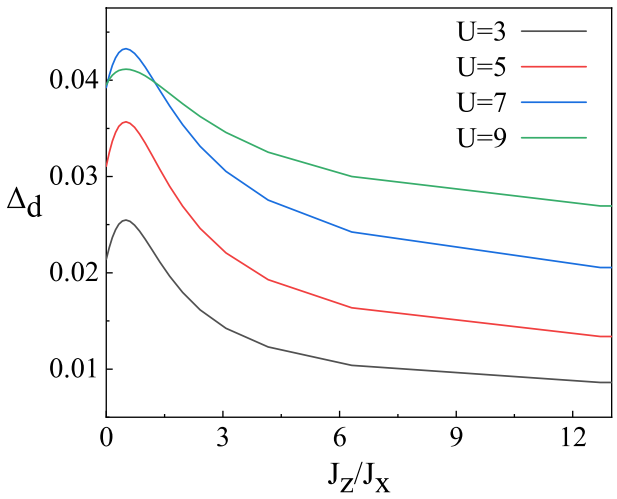

Figure 7. d-wave order parameter Δ_d at half-filling for several values of U.

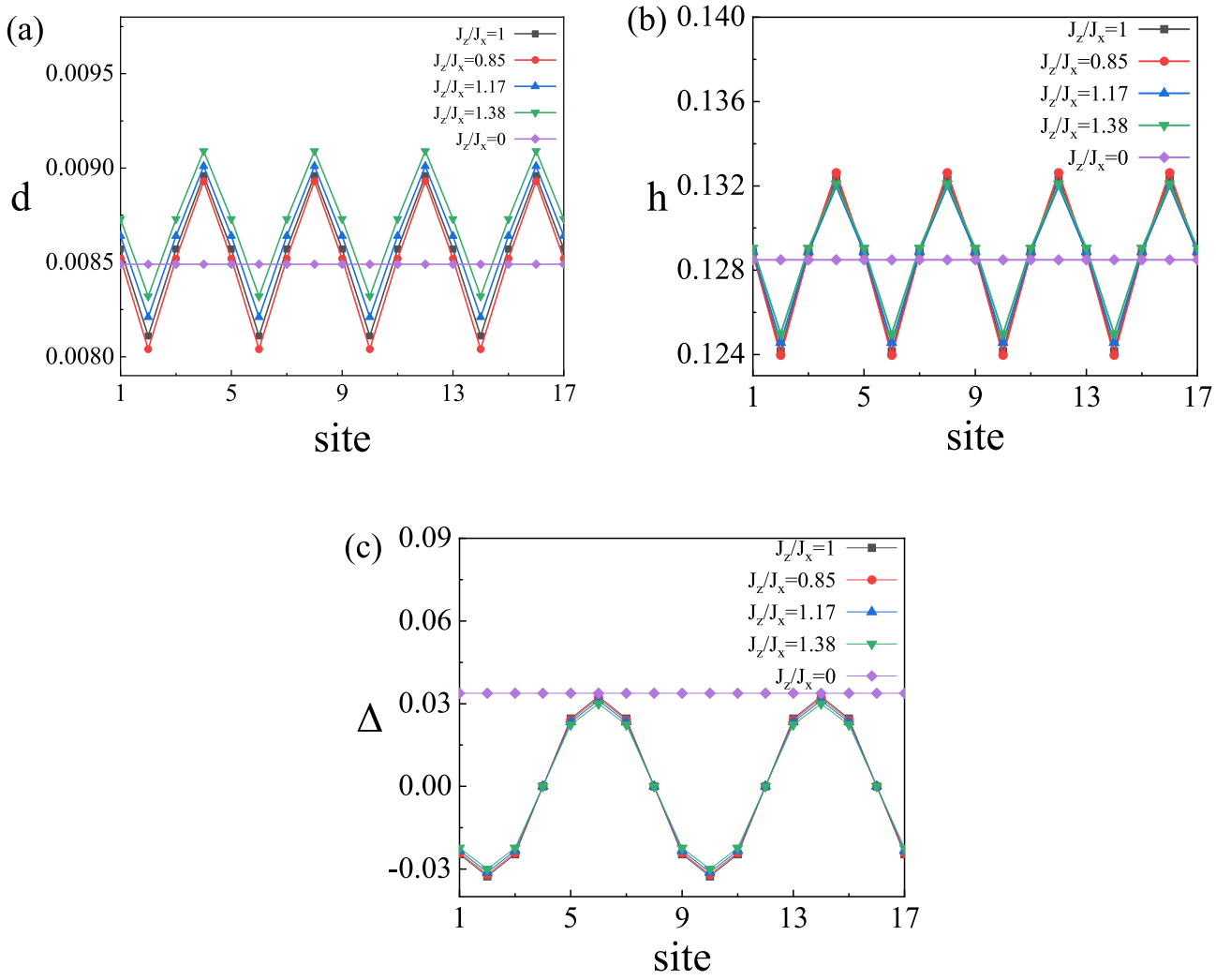

Figure 8. Features of the AP-CDW state at $U = 15$ and $\delta = 0.12$ with lattice sites 1–17 in x direction. (**a**) Variation of doublon density in the system. (**b**) Variation of hole density in the system. (**c**) Variation of the superconducting order parameter in the system.

range. In the two anisotropic models, it is similar that the anisotropy will limit the size of the pairing field, and then affect the formation of the gap. In the large U area, antiferromagnetic interaction anisotropy has little effect on the amplitude of charge-ordered states. All charge-ordered states are suppressed in the limit case, leaving only uniform states. Both types of anisotropy will suppress the charge fluctuations. Therefore, the t–J–U model with hopping anisotropy can represent the essential physics of YBCO materials.

Methods

We study two anisotropic t–J–U models, hopping anisotropy and antiferromagnetic interaction anisotropy. The t–J–U model with hopping anisotropy on a square lattice is given by

$$H = -\sum_{i\sigma}\left(t_x c^{\dagger}_{i+x\sigma}c_{i\sigma} + t_y c^{\dagger}_{i+y\sigma}c_{i\sigma} + \text{H.c.}\right) + J\sum_{\langle ij\rangle}\boldsymbol{S_i}\cdot\boldsymbol{S_j} + U\sum_i n_{i\uparrow}n_{i\downarrow}. \tag{1}$$

where t_x and t_y are the hopping matrix element between the nearest neighbor in the x and y direction. The average of nearest-neighbor hopping $(t_x + t_y)/2$, as our energy unit, is set to 1. J term is the Heisenberg interaction between the nearest neighbor and is set to $J = 1/3$. $c_{i\sigma}$ is electron annihilation operator with spin $\sigma = \pm$ at site i and $\boldsymbol{S_i}$ is the spin-1/2 operator. $U > 0$ is on-site Coulomb repulsion.

The t–J–U model with antiferromagnetic interaction anisotropy on a square lattice is given by

$$H = -\sum_{\langle ij\rangle,\sigma} t\left(c^{\dagger}_{i\sigma}c_{j\sigma} + \text{H.c.}\right) + \sum_{\langle ij\rangle}\left(\frac{J_x}{2}S^{+}_i S^{-}_j + \frac{J_x}{2}S^{-}_i S^{+}_j + J_z S^{z}_i S^{z}_j\right) + U\sum_i n_{i\uparrow}n_{i\downarrow}. \tag{2}$$

where t term denotes the nearest-neighbor hopping matrix element, and it is set to be the energy unit. The nearest-neighbor antiferromagnetic Heisenberg interaction $J_x(J_z)$ satisfy $J_x^2 + J_z^2 = (1/3)^2$.

We take a partially projected variational trial wave function proposed by Laughlin[54]

$$|\Psi_{GS}\rangle = \prod_{\alpha} |\Psi_0\rangle, \tag{3}$$

$$\prod_{\alpha} = \prod_{i} (1 - \alpha n_{i\uparrow} n_{i\downarrow}). \tag{4}$$

where $|\Psi_0\rangle$ is BCS superconducting state, and $\prod_\alpha$ is the projection operator, which partially projects out double occupancy on each site. $|\Psi_{GS}\rangle$ smoothly connects the BCS state with the RVB state. $\alpha = 0$ represents the BCS state and $\alpha = 1$ corresponds to the RVB state.

The projection operator incorporates strong electron correlations, which can be handled by the Gutzwiller approximation method, which considers the effect of projection through a set of statistical weight factors. Then the hopping term and the Heisenberg interaction in the partially projected state and unprojected BCS state are related by Gutzwiller renormalization factors

$$\begin{aligned} \left\langle c_{i\sigma}^{\dagger} c_{j\sigma} \right\rangle &= g_{ij}^{t} \left\langle c_{i\sigma}^{\dagger} c_{j\sigma} \right\rangle_0, \\ \left\langle \boldsymbol{S_i} \cdot \boldsymbol{S_j} \right\rangle &= g_{ij}^{s} \left\langle \boldsymbol{S_i} \cdot \boldsymbol{S_j} \right\rangle_0. \end{aligned} \tag{5}$$

The Gutzwiller renormalization factors on each site are given as

$$\begin{aligned} g_{ij}^{t} &= g_i^{t} g_j^{t}, \\ g_i^{t} &= \frac{\sqrt{n_i - 2d_i}\left(\sqrt{d_i} + \sqrt{1 - n_i + d_i}\right)}{\sqrt{\left(1 - \frac{n_i}{2}\right) n_i}}, \\ g_{ij}^{s} &= g_i^{s} g_j^{s}, \\ g_i^{s} &= \frac{n_i - 2d_i}{\left(1 - \frac{n_i}{2}\right) n_i}. \end{aligned} \tag{6}$$

In terms of these renormalization factors, the renormalized Hamiltonian can be obtained as

$$H' = -\sum_{i\sigma} \left(g_{ii+x}^{t} t_x c_{i+x\sigma}^{\dagger} c_{i\sigma} + g_{ii+y}^{t} t_y c_{i+y\sigma}^{\dagger} c_{i\sigma} + \text{H.c.} \right) + \sum_{\langle ij \rangle} g_{ij}^{s} \left(\frac{J_x}{2} S_i^{+} S_j^{-} + \frac{J_x}{2} S_i^{-} S_j^{+} + J_z S_i^{z} S_j^{z} \right) + U \sum_{i} n_{i\uparrow} n_{i\downarrow}. \tag{7}$$

Thus the ground-state energy in the state $|\Psi_{GS}\rangle$ can be evaluated by the expectation of H' in the BCS state $|\Psi_0\rangle$

$$E = \left\langle H' \right\rangle_0 = U \sum_{i} d_i + g_t \langle H_t \rangle_0 + g_s \left\langle H_J \right\rangle_0. \tag{8}$$

Local electron density and local pairing field, and local bond field are defined as

$$\begin{aligned} n_i &= \left\langle \Psi_0 \middle| c_{i\uparrow}^{\dagger} c_{i\uparrow} + c_{i\downarrow}^{\dagger} c_{i\downarrow} \middle| \Psi_0 \right\rangle = 1 - \delta_i, \\ \Delta_{ij\sigma}^{v} &= \sigma \left\langle \Psi_0 \middle| c_{i\sigma} c_{j\bar{\sigma}} \middle| \Psi_0 \right\rangle, \\ \chi_{ij\sigma}^{v} &= \left\langle \Psi_0 \middle| c_{i\sigma}^{\dagger} c_{j\sigma} \middle| \Psi_0 \right\rangle. \end{aligned} \tag{9}$$

The d-wave and s-wave superconducting gap can be given by the pairing fields and renormalization factors as

$$\Delta_i^{d} = \frac{1}{8} \sum_{\sigma} \left(g_{i,i+\hat{x}}^{t} \Delta_{i,i+\hat{x},\sigma}^{v} + g_{i,i-\hat{x}}^{t} \Delta_{i,i-\hat{x},\sigma}^{v} - g_{i,i+\hat{y}}^{t} \Delta_{i,i+\hat{y},\sigma}^{v} - g_{i,i-\hat{y}}^{t} \Delta_{i,i-\hat{y},\sigma}^{v} \right). \tag{10}$$

$$\Delta_i^{s} = \frac{1}{8} \sum_{\sigma} \left(g_{i,i+\hat{x}}^{t} \Delta_{i,i+\hat{x},\sigma}^{v} + g_{i,i-\hat{x}}^{t} \Delta_{i,i-\hat{x},\sigma}^{v} + g_{i,i+\hat{y}}^{t} \Delta_{i,i+\hat{y},\sigma}^{v} + g_{i,i-\hat{y}}^{t} \Delta_{i,i-\hat{y},\sigma}^{v} \right). \tag{11}$$

The ground-state energy can be expressed by the parameters as

$$E = -\sum_{\langle ij \rangle,\sigma} g_{ij}^{t} t_{ij} \left(\chi_{ij\sigma}^{v} + \text{H.c.} \right) - \sum_{\langle ij \rangle,\sigma} \frac{3}{4} J g_{ij}^{s} \Delta_{ij\sigma}^{v*} \Delta_{ij\sigma}^{v} - \sum_{\langle ij \rangle,\sigma} \frac{3}{4} J g_{ij}^{s} \chi_{ij\sigma}^{v*} \chi_{ij\sigma}^{v} + U \sum_{i} d_i \tag{12}$$

And a mean-field Hamiltonian can be expressed as

$$H_{MF} = \sum_{(ij),\sigma} \varepsilon_{ij\sigma} c_{i\sigma}^{\dagger} c_{j\sigma} + \text{H.c.} + \sum_{\langle ij \rangle,\sigma} \sigma D_{ij\sigma}^{*} c_{i\sigma} c_{j\bar{\sigma}} + \text{H.c.} - \sum_{i,\sigma} \mu_{i\sigma} n_{i\sigma} \tag{13}$$

The coefficients are given as

$$\begin{aligned}\varepsilon_{ij\sigma} &= -\frac{3}{4}Jg_{ij}^{s}\chi_{ij\sigma}^{v*} - g_{ij}^{t}t_{ij},\\ D_{ij\sigma}^{*} &= -\frac{3}{4}Jg_{ij}^{s}\Delta_{ij\sigma}^{v*},\\ \mu_{i\sigma} &= \mu - \sum_{j}\left(\frac{\partial W}{\partial g_{ij}^{s}}\frac{\partial g_{ij}^{s}}{\partial n_{i\sigma}} + \frac{\partial W}{\partial g_{ij}^{t}}\frac{\partial g_{ij}^{t}}{\partial n_{i\sigma}}\right).\end{aligned} \tag{14}$$

A Bogoliubov–de Gennes (BdG) equation can solve the above Hamiltonian. Local doublon density is determined by the minimization of the ground-state energy

$$\frac{\partial E}{\partial d_i} = U + \sum_{j}\left(\frac{\partial W}{\partial g_{ij}^{s}}\frac{\partial g_{ij}^{s}}{\partial d_i} + \frac{\partial W}{\partial g_{ij}^{t}}\frac{\partial g_{ij}^{t}}{\partial d_i}\right) = 0. \tag{15}$$

The LDOS can be computed by the eigenvalues E_n and eigenvectors (u_i^n, v_i^n) of the BdG equation

$$\rho_i(E) = \left(g_i^t\right)^2 \sum_{n}\left[\left|u_i^n\right|^2\delta(E - E_n) + \left|v_i^n\right|^2\delta(E + E_n)\right]. \tag{16}$$

All the local order parameters are solved self-consistently. The system size we take is 64×64. First, we input initial values to the electron density and doublon density on each site, bond field, and pairing field on each nearest-neighbor bond. Then we solve the BdG equations and calculate all the order parameters. Iterate the above process until the relative changes between the last two order parameters is less than 10^{-4}.

Data availability

The data used to support the findings of this study are included in the article.

Received: 6 May 2023; Accepted: 9 January 2024
Published online: 16 January 2024

References

1. Lee, P. A., Nagaosa, N. & Wen, X.-G. Doping a mott insulator: Physics of high-temperature superconductivity. *Rev. Mod. Phys.* **78**, 17–85 (2006).
2. Fradkin, E., Kivelson, S. A. & Tranquada, J. M. Colloquium: Theory of intertwined orders in high temperature superconductors. *Rev. Mod. Phys.* **87**, 457–482 (2015).
3. Daou, R. *et al.* Broken rotational symmetry in the pseudogap phase of a high-T_c superconductor. *Nature* **463**, 519–522 (2010).
4. Chang, J. *et al.* Nernst effect in the cuprate superconductor $YBa_2Cu_3O_y$: Broken rotational and translational symmetries. *Phys. Rev. B* **84**, 014507 (2011).
5. Ando, Y., Segawa, K., Komiya, S. & Lavrov, A. N. Electrical resistivity anisotropy from self-organized one dimensionality in high-temperature superconductors. *Phys. Rev. Lett.* **88**, 137005 (2002).
6. Hinkov, V. *et al.* Electronic liquid crystal state in the high-temperature superconductor $YBa_2Cu_3O_{6.45}$. *Science* **319**, 597–600 (2008).
7. Lu, D. H. *et al.* Superconducting gap and strong in-plane anisotropy in untwinned $YBa_2Cu_3O_{7-\delta}$. *Phys. Rev. Lett.* **86**, 4370–4373 (2001).
8. Okawa, M. *et al.* Superconducting electronic state in optimally doped $YBa_2Cu_3O_{7-\delta}$ observed with laser-excited angle-resolved photoemission spectroscopy. *Phys. Rev. B* **79**, 144528 (2009).
9. Bakr, M. *et al.* Electronic and phononic raman scattering in detwinned $YBa_2Cu_3O_{6.95}$ and $Y_{0.85}Ca_{0.15}Ba_2Cu_3O_{6.95}$: *s*-wave admixture to the $d_{x^2-y^2}$-wave order parameter. *Phys. Rev. B* **80**, 064505 (2009).
10. Kirtley, J. R. *et al.* Angle-resolved phase-sensitive determination of the in-plane gap symmetry in $YBa_2Cu_3O_{7-\delta}$. *Nature Physics* **2**, 190–194 (2006).
11. Smilde, H. J. H. *et al.* Admixtures to *d*-wave gap symmetry in untwinned $YBa_2Cu_3O_7$ superconducting films measured by angle-resolved electron tunneling. *Phys. Rev. Lett.* **95**, 257001 (2005).
12. Ghiringhelli, G. *et al.* Long-range incommensurate charge fluctuations in (Y, Nd)$Ba_2Cu_3O_{6+x}$. *Science* **337**, 821–825 (2012).
13. Achkar, A. J. *et al.* Distinct charge orders in the planes and chains of ortho-III-ordered $YBa_2Cu_3\mathbf{O}_{6+\delta}$ superconductors identified by resonant elastic X-ray scattering. *Phys. Rev. Lett.* **109**, 167001 (2012).
14. Blanco-Canosa, S. *et al.* Momentum-dependent charge correlations in $YBa_2Cu_3O_{6+\delta}$ superconductors probed by resonant X-ray scattering: Evidence for three competing phases. *Phys. Rev. Lett.* **110**, 187001 (2013).
15. Chang, J. *et al.* Direct observation of competition between superconductivity and charge density wave order in $YBa_2Cu_3O_{6.67}$. *Nature Physics* **8**, 871–876 (2012).
16. Blackburn, E. *et al.* X-ray diffraction observations of a charge-density-wave order in superconducting ortho-II $YBa_2Cu_3\mathbf{O}_{6.54}$ single crystals in zero magnetic field. *Phys. Rev. Lett.* **110**, 137004 (2013).
17. Hücker, M. *et al.* Competing charge, spin, and superconducting orders in underdoped $YBa_2Cu_3O_y$. *Phys. Rev. B* **90**, 054514 (2014).
18. LeBoeuf, D. *et al.* Thermodynamic phase diagram of static charge order in underdoped YBa_2Cu3O_y. *Nature Physics* **9**, 79–83 (2013).
19. Yamada, K. *et al.* Doping dependence of the spatially modulated dynamical spin correlations and the superconducting-transition temperature in $La_{2-x}Sr_xCuO_4$. *Phys. Rev. B* **57**, 6165–6172 (1998).
20. Wu, H. H. *et al.* Charge stripe order near the surface of 12-percent doped $La_{2-x}Sr_xCuO_4$. *Nature Communications* **3**, 1023 (2012).
21. Croft, T. P., Lester, C., Senn, M. S., Bombardi, A. & Hayden, S. M. Charge density wave fluctuations in $La_{2-x}Sr_xCuO_4$ and their competition with superconductivity. *Phys. Rev. B* **89**, 224513 (2014).
22. Hücker, M. *et al.* Stripe order in superconducting $La_{2-x}Ba_xCuO_4$ ($0.095 \leqslant x \leqslant 0.155$). *Phys. Rev. B* **83**, 104506 (2011).
23. Wen, J. J. *et al.* Observation of two types of charge-density-wave orders in superconducting $La_{2-x}Sr_xCuO_4$. *Nature Communications* **10**, 3269 (2019).
24. Corboz, P., Rice, T. M. & Troyer, M. Competing states in the *t*-*J* model: Uniform *d*-wave state versus stripe state. *Phys. Rev. Lett.* **113**, 046402 (2014).

25. Zhang, F. C. & Rice, T. M. Effective hamiltonian for the superconducting Cu oxides. *Phys. Rev. B* **37**, 3759–3761 (1988).
26. Zhang, F. C., Gros, C., Rice, T. M. & Shiba, H. A renormalised hamiltonian approach to a resonant valence bond wavefunction. *Superconductor Science and Technology* **1**, 36–46 (1988).
27. Tu, W.-L. & Lee, T.-K. Genesis of charge orders in high temperature superconductors. *Scientific Reports* **6**, 18675 (2016).
28. Raczkowski, M., Capello, M., Poilblanc, D., Frésard, R. & Oleś, A. M. Unidirectional *d*-wave superconducting domains in the two-dimensional $t - J$ model. *Phys. Rev. B* **76**, 140505 (2007).
29. Yang, K.-Y., Chen, W. Q., Rice, T. M., Sigrist, M. & Zhang, F.-C. Nature of stripes in the generalized t-J model applied to the cuprate superconductors. *New Journal of Physics* **11**, 055053 (2009).
30. Choubey, P., Tu, W.-L., Lee, T.-K. & Hirschfeld, P. J. Incommensurate charge ordered states in the t-t'-J model. *New Journal of Physics* **19**, 013028 (2017).
31. Tu, W.-L. & Lee, T.-K. Evolution of pairing orders between pseudogap and superconducting phases of cuprate superconductors. *Scientific Reports* **9**, 1719 (2019).
32. Daul, S., Scalapino, D. J. & White, S. R. Pairing correlations on $t-U-J$ ladders. *Phys. Rev. Lett.* **84**, 4188–4191 (2000).
33. Zhang, F. C. Gossamer superconductor, mott insulator, and resonating valence bond state in correlated electron systems. *Phys. Rev. Lett.* **90**, 207002 (2003).
34. Guertler, S., Wang, Q.-H. & Zhang, F.-C. Variational Monte Carlo studies of Gossamer superconductivity. *Phys. Rev. B* **79**, 144526 (2009).
35. Gan, J. Y., Chen, Y. & Zhang, F. C. Superconducting pairing symmetries in anisotropic triangular quantum antiferromagnets. *Phys. Rev. B* **74**, 094515 (2006).
36. Hou, J., Lee, T.-K., Lou, J. & Chen, Y. Charge-ordered states in the $t-J-U$ model. *Phys. Rev. B* **100**, 144516 (2019).
37. Nocera, A., Patel, N. D., Dagotto, E. & Alvarez, G. Signatures of pairing in the magnetic excitation spectrum of strongly correlated two-leg ladders. *Phys. Rev. B* **96**, 205120 (2017).
38. Spałek, J., Zegrodnik, M. & Kaczmarczyk, J. Universal properties of high-temperature superconductors from real-space pairing: $t-J-U$ model and its quantitative comparison with experiment. *Phys. Rev. B* **95**, 024506 (2017).
39. Spałek, J., Fidrysiak, M., Zegrodnik, M. & Biborski, A. Superconductivity in high-T_c and related strongly correlated systems from variational perspective: Beyond mean field theory. *Physics Reports* **959**, 1–117 (2022).
40. Atkinson, W. A. Disorder and chain superconductivity in $YBa_2Cu_3O_{7-\delta}$. *Phys. Rev. B* **59**, 3377–3380 (1999).
41. Morr, D. K. & Balatsky, A. V. Proximity effects and quantum dissipation in the chains of $YBa_2Cu_3O_{6+x}$. *Phys. Rev. Lett.* **87**, 247002 (2001).
42. Das, T. In-plane anisotropy in spin-excitation spectra originating from chain states in $YBa_2Cu_3O_{6+y}$. *Phys. Rev. B* **85**, 144510 (2012).
43. Das, T. Electron-like fermi surface and in-plane anisotropy due to chain states in $YBa_2Cu_3O_{7-\delta}$ superconductors. *Phys. Rev. B* **86**, 064527 (2012).
44. Pasanai, K. & Atkinson, W. A. Theory of (001) surface and bulk states in $Y_{1-y}Ca_yBa_2Cu_3O_{7-\delta}$. *Phys. Rev. B* **81**, 134501 (2010).
45. Yamase, H. & Kohno, H. Instability toward formation of quasi-one-dimensional fermi surface in two-dimensional t-J model. *Journal of the Physical Society of Japan* **69**, 2151–2157 (2000).
46. Basu, S., Gooding, R. J. & Leung, P. W. Enhanced bound-state formation in two dimensions via stripelike hopping anisotropies. *Phys. Rev. B* **63**, 100506 (2001).
47. Basu, S., Callan-Jones, A. & Gooding, R. J. Increasing superconducting T_c's by a factor of 1000 with large hopping anisotropies in two-dimensional $t-J$ model systems. *Phys. Rev. B* **66**, 144507 (2002).
48. Kampf, A. P., Scalapino, D. J. & White, S. R. Stripe orientation in an anisotropic $t-J$ model. *Phys. Rev. B* **64**, 052509 (2001).
49. Becca, F., Capriotti, L. & Sorella, S. Stripes and spin incommensurabilities are favored by lattice anisotropies. *Phys. Rev. Lett.* **87**, 167005 (2001).
50. Miyanaga, A. & Yamase, H. Orientational symmetry-breaking correlations in square lattice t-J model. *Phys. Rev. B* **73**, 174513 (2006).
51. Zegrodnik, M., Biborski, A. & Spałek, J. Superconductivity and intra-unit-cell electronic nematic phase in the three-band model of cuprates. *The European Physical Journal B* **93**, 183 (2020).
52. Guguchia, Z. *et al.* Using uniaxial stress to probe the relationship between competing superconducting states in a cuprate with spin-stripe order. *Phys. Rev. Lett.* **125**, 097005 (2020).
53. Gupta, N. K. *et al.* Tuning charge density wave order and structure via uniaxial stress in a stripe-ordered cuprate superconductor. *Phys. Rev. B* **108**, L121113 (2023).
54. Laughlin, R. B. Gossamer superconductivity. *Philosophical Magazine* **86**, 1165–1171 (2006).

Acknowledgements

This work was supported by the National Key Research and Development Program of China Grant No. 2022YFA1404204, and the National Natural Science Foundation of China (Grants No. 11625416 and No. 12274086).

Author contributions

All authors wrote and reviewed the manuscript.

Competing interests

The authors declare no competing interests.

Additional information

Correspondence and requests for materials should be addressed to Y.C.

Reprints and permissions information is available at www.nature.com/reprints.

Publisher's note Springer Nature remains neutral with regard to jurisdictional claims in published maps and institutional affiliations.